ChemPubSoc Europe

DOI: 10.1002/chem.201800500

CHEMISTRY A European Journal Full Paper

Systems Chemistry

Functional Assemblies Emerging in Complex Mixtures of Peptides and Nucleic Acid–Peptide Chimeras

Agata Chotera,[a] Hava Sadihov,[a] Rivka Cohen-Luria,[a] Pierre-Alain Monnard,[b] and Gonen Ashkenasy*[a]

Abstract: Striking synergy between nucleic acids and proteins is exhibited in living cells. Whether such mutual activity can be performed using simple supramolecular nucleic acid–peptide (NA-pep) architectures remains a mystery. To shed light on this question, we studied the emergence of a primitive synergy in assemblies of short DNA-peptide chimeras. Specifically, we characterized multiple structures forming along gradual mixing trajectory, in which a peptide solution was seeded with increasing amounts of NA-pep chimeras. We report on the systematic change from β-sheet-peptide-based fibrillar architectures into the spherical structures formed by the conjugates. Remarkably, we find that through forming onion-like structures, the conjugates exhibit increased DNA hybridization stability and bind small molecules more efficiently than the peptides or DNA alone. A brief discussion highlights the implications of our findings for the production of new materials and for research on the origin of life.

Introduction

The enormously diverse biochemistry in living cells is made possible by molecules from a small number of families, primarily proteins, nucleic acids, fatty acids and sugars. While simple operations, such as catalysis of a specific chemical transformation, involve a single (enzyme) molecule or a small complex of identical molecules, more elaborate tasks are often driven by synergistic activity in assemblies of interacting molecules from different families. Two major examples of such synergy between nucleic acids and proteins are the specific protein synthesis by the ribosome that translates RNA sequences,[1] and RNA (or DNA) assembly and packaging by proteins in virus particles, which control the entire viral replication cycle.[2] The emergence of a primitive synergy in assemblies of much simpler nucleic acid–peptide (NA-pep) chimeras is the topic of the current paper. We posited that covalent interactions between short nucleic acid and peptide segments and spontaneous assembly of the chimeras will yield new structures based on both the peptide association and sequence-specific hybridization of the oligonucleotides.[3] We furthermore hypothesized that these assemblies would be superior, in terms of structure stability and function, to their peptide-only or nucleic-acid-only counterparts.

To address the above hypotheses, we prepared two novel DNA–peptide conjugates (**DNA1-pep** and **DNA2-pep**, Figure 1) and studied their assembly along a putative mixing trajectory, in which a solution containing peptide molecules was seeded with increasing amounts of one of the conjugates (ssCon) or with pre-hybridized two conjugates (dsCon). In this paper, we report a remarkable step-by-step morphological transition, leading from β-sheet peptide-dominated fibrillar architectures into dsCon-based spherical, densely packed structures formed

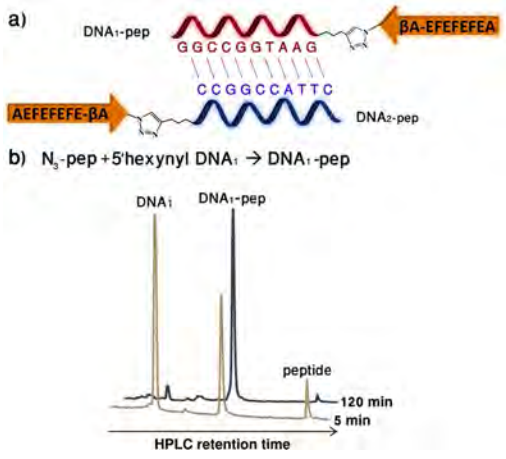

Figure 1. DNA-pep chimeras. a) DNA-pep sequences, highlighting the complementary nature of the DNA segments and the β-strand formed by the peptide segments. Single-letter nomenclature is used to represent the sequences. βA = β-alanine. b) HPLC and MALDI-TOF MS characterization of **DNA1-pep** during 2 h of a "click" reaction between the N_3-pep and 5′-hexynyl precursors. Figure S1 shows a similar characterization of the **DNA2-pep** conjugate.

[a] *A. Chotera, H. Sadihov, Dr. R. Cohen-Luria, Prof. G. Ashkenasy*
Department of Chemistry, Ben-Gurion University of the Negev
Beer-Sheva 84105 (Israel)
E-mail: gonenash@bgu.ac.il

[b] *Prof. P.-A. Monnard*
Institute for Physics, Chemistry and Pharmacy
University of Southern Denmark, 5230 Odense M (Denmark)

Supporting information and the ORCID identification number for the author of this article can be found under: https://doi.org/10.1002/chem.201800500.

by concentric bilayers. A set of experiments allows us to propose an interaction model for the production of such spheres. Finally, we reveal that through the formation of spherical particles, dsCon exhibits increased stability towards elevated temperatures and pH values and can efficiently and reversibly bind to small molecules, such as the dye thioflavin T (ThT) and the drug doxorubicin (Dox).

Results and Discussion

DNA1-pep and **DNA2-pep** conjugates contain segments of ten nucleotides attached through a short triazole-based linker to an amphiphilic peptide of nine amino acids (Figure 1). The DNA domains of the two conjugates are complementary to each other. Each molecule contains a non-palindromic NA sequence and a low ratio of guanine (G) bases in order to limit the formation of undesired structures. In addition, these two sequences are presumably too short to form a very stable duplex without auxiliary interactions, such as those facilitated by conjugation to the peptide. The peptide domain sequence derived from related molecules previously studied by our group, containing repetitive Glu–Phe dyads. As observed for other short amphiphilic peptides,[4] the Glu–Phe peptides can readily assemble into β-sheet fibrils[5] and function as catalysts,[6] replicators,[7] and even as charge transport entities.[8] The oligonucleotide and peptide segments were prepared separately by solid phase synthesis, and each segment was functionalized to be linked together by a copper(II)-catalyzed "click" reaction (Figure 1).[9] After conjugation, **DNA1-pep** and **DNA2-pep** were purified, and their purity and molecular weights were characterized by HPLC and MALDI-TOF MS (Figures 1b and S1).

Assemblies formed by the peptide molecules alone (N_3-pep) were characterized first with the aim to detect structure(s) likely to form later on in mixtures with the DNA-pep conjugates. TEM and AFM images revealed straight fibril-like structures that were closely associated and bundled one next to the other (Figure 2). The width of these fibrils, around 4 nm, correlates well with a bilayer packing where Phe side chains are hidden within the hydrophobic fibril core, as we have previously observed for related peptides.[5a,8b] Further characterization by CD (Figure S2) and FTIR (Figure S3) revealed the typical characteristics of β-sheet structures, including the amide bond IR absorbance peaks at 1623 and 1694 cm^{-1}, indicating the formation of antiparallel sheets.

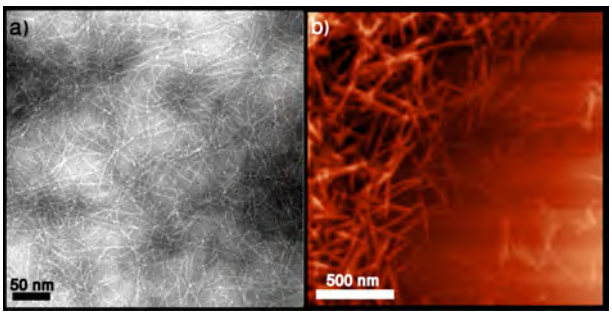

Figure 2. N_3-pep fibril assembly structures formed in aqueous solutions at pH 7 and characterized by TEM (a, 500 μM) and AFM (b, 50 μM).

Structure formation in mixtures (50 μM total concentration each) containing either N_3-pep and a single type of conjugate ssCon or N_3-pep and the hybridized complementary conjugate dsCon was then followed extensively by AFM and cryo-TEM (Figure 3). We note that N_3-pep and both the DNA and peptide segments of **DNA1-pep** and **DNA2-pep** are all negatively charged at neutral pH, implying that their mutual assembly is driven primarily by peptide-peptide interactions and inter-molecular, H-bonding directed, hybridization of nucleic acid segments. AFM images obtained for the assemblies formed in mixtures of N_3-pep and low concentrations of **DNA1-pep** showed narrow and bundled fibril assemblies (Figure 3a), similar to the fibrils formed by N_3-pep alone. Images obtained for mixtures with a higher ssCon/pep ratio (1:1) revealed the formation of around 50% wider and more flexible (curved) fibrils with larger distances from one another (Figure 3b), probably since solvent-exposed DNA segments limited their association. While under these conditions individual fibrils were found (marked as 1 in Figure 3b), the fibril length varied significantly (150 nm up to a few microns), and inter-fibril association also led to bundled morphologies of different width (Figure 3b; 2 and 3). Consistently, **DNA1-pep** or **DNA2-pep** molecules alone also formed bundled architectures (AFM; Figure S4a and S4c), or rather shorter fibrils at higher concentrations (cryo-TEM; Figure S4b).

Structure formation in mixtures containing N_3-pep and different amounts of **DNA1-pep** and **DNA2-pep** conjugates (1:1 ratio) was directed by first dissolving all three components in buffer (pH 7; 10 mM Mg^{2+}), incubating the mixture at $\geq 70\,^{\circ}C$ (10 min), and then cooling it to RT for a further incubation of at least 3 h. Spatially isolated, apparently linear and stiff, fibril assemblies were formed in mixtures containing N_3-pep and low molar fractions of dsCon (Figure 3c,d). Remarkably different structures were found in mixtures of N_3-pep and higher molar fractions of the **DNA1-pep** and **DNA2-pep** conjugates (1:1:1), namely, co-assembly architectures composed of a fibril-like skeleton decorated with spherical objects (Figures 3e and S5). A similar "beads-on-a-string" configuration was previously obtained for the co-assembly of two peptides having different hydrophobicity.[10] Close inspection of the newly formed architectures showed that all the fiber elements were of similar width (≈4 nm) and that they were sometimes bundled to wider aggregates. Current data resolution allows us to propose that fiber and sphere elements are bound through inter-assembly DNA hybridization, and/or overlapping hydrophobic interactions between β-sheet peptide segments. We further note that isolated spheres can also form under these conditions, supposedly made of only (or largely) the dsCon duplexes, as discussed in detail in the following.

To examine the final stage of this gradual mixing course, we characterized the assembly products obtained after annealing and equilibration of the two complementary conjugates **DNA1-pep** and **DNA2-pep** (25 μM each, $[N_3\text{-pep}] = 0$; Figure 4). Cryo-TEM measurements (Figure 4a and Figure 4c), and dry TEM measurements (Figure 4d, Figures 4e and S8) revealed

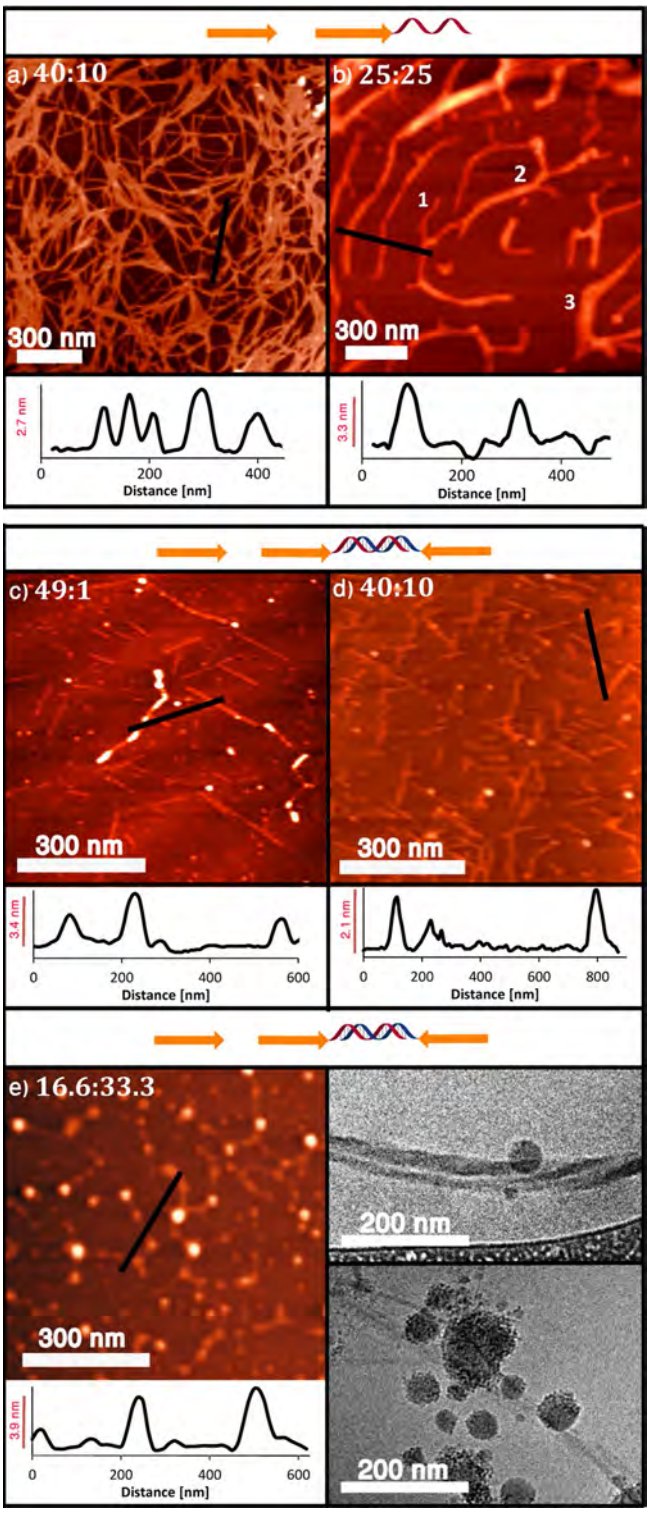

Figure 3. AFM and cryo-TEM images of self-assembled nanostructures formed in mixtures containing either N_3-pep and ssCon [**DNA1-pep**; (a, b)] or N_3-pep and dsCon (c–e). Traces below the AFM images show the respective height cross-sections. Numbers 1–3 in panel b highlight the formation of individual fibrils and fibril bundles of variable width. The structures were formed in mixtures of 50 μM total concentration; the ratio between peptide and conjugate(s) is given in each panel (e.g., in panel d, '40:10' represents 40 μM N_3-pep mixed together with 5 μM **DNA1-pep** and 5 μM **DNA2-pep**). Additional images are given in Figures S4 and S5.

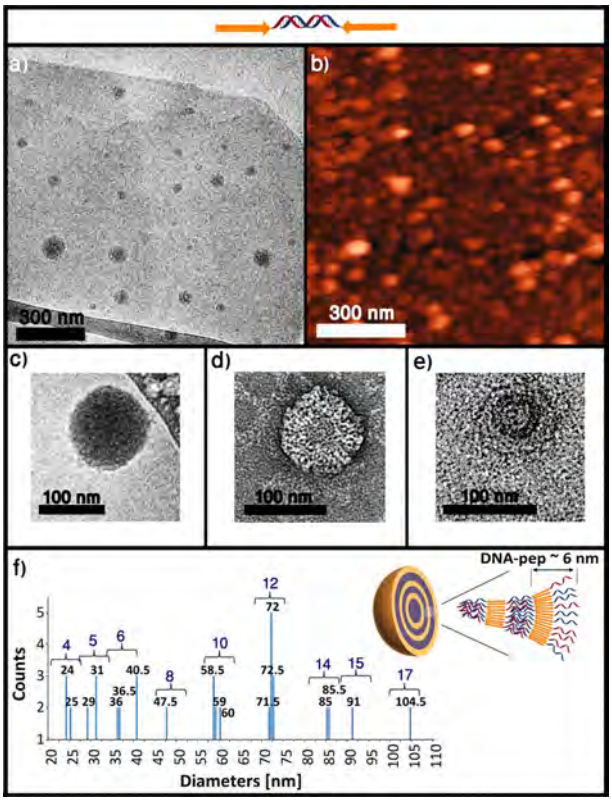

Figure 4. Characterization of the spherical assemblies formed by pure dsCon. a) Cryo-TEM images. b) AFM images. c) Enlarged image of an individual sphere observed in the Cryo-TEM measurements. d, e) Enlarged images of individual spheres observed in dry TEM measurements; data collected after staining with uranyl acetate. Additional images of dsCon spheres are given in Figures S8 and S12. f) Statistical analysis using differential count of sphere diameters (bin = 0.5 nm; count numbers ≥ 2). Values in blue refer to the number of layers in the corresponding group of spherical assemblies, calculated for the assumed round figure of 6 nm per layer (see scheme at the top right of this panel).

the formation of rounded crowded spheres with diameters ranging 20–180 nm. Likewise, DLS characterization of the 50 μM dsCon revealed the formation of particles 20–80 nm in radius (mean radius = 37 nm, Figure S6), and DLS of a much more concentrated sample (500 μM) showed only slightly larger aggregates (mean radius = 51 nm, Figure S6). Analysis of the AFM data (Figures 4b and S7) indicated rather flat aggregates, shorter in the *z* direction (19 nm in average) than in their lateral diameter (130 nm), suggesting that the spheres had shrunk upon drying on the mica surfaces and/or that the images had been subject to the AFM tip convolution effect. Statistical analysis of an ensemble of the cryo-TEM images revealed that dsCon formed spherical architectures with distinct diameter values (Figures 4f, S9 and S10). We therefore grouped together structures of similar size, representing spheres with distinct numbers of DNA-pep layers, when taking into account that the assembly of each layer expands its diameter by ≈6 nm. Remarkably, we indeed found narrow diameter distributions, centering close to the predicted value for each of the sphere groups (Figure 4f).

Further insight into the dsCon molecular arrangement within the spheres was obtained from the higher resolution

TEM data in Figures 4e and S8, allowing to detect "rings" for the different assembly layers. CD measurements (Figure S11), in addition showed that the DNA segments in dsCon primarily took the more compact B-form,[11] unlike dsDNA of the same sequences, which in control studies formed mostly A-type helix structures, as typically observed for short G-C-rich sequences.[11b] Taken together, our results indicate the formation of multi-lamellar spherical architectures (Figure 4f, inset), as was previously observed for related assemblies formed by Janus soft-matter building blocks,[12] such as lipid-DNA molecules.[13]

Several recently published works have described the self-assembly of NA-pep conjugates into vesicle or fibril-like architectures. In such studies, scientist have characterized assemblies formed by NA moieties attached to either short peptides[14] or to positively charged peptides that strongly interact intramolecularly with the NA segments.[15] Co-assembly via noncovalent association of positively charged peptides (or proteins) and NA polymers have also been disclosed recently.[16] The chimeras introduced here produce a different type of assembly, in which minimal interaction takes place between DNA and the peptide domains of the same molecules, implying that new architectures are formed on the basis of synergy, due to a collective set of interactions. Most remarkably, to the best of our knowledge, this is the first systematic study showing the gradual change from peptide fibrils to conjugate multi-lamellar spheres, while also isolating the intermediate architectures formed along the way (Scheme 1). In order to directly probe

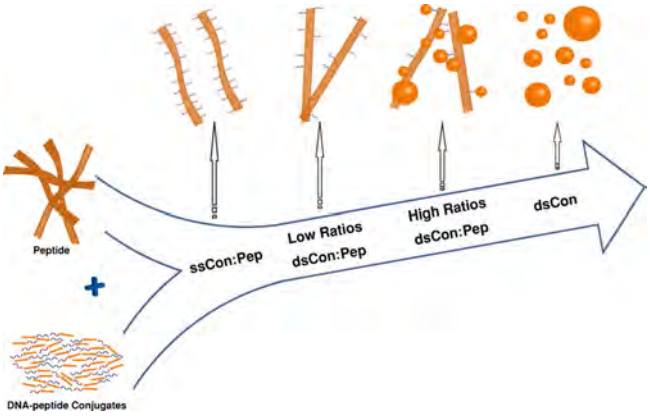

Scheme 1. Gradual structural changes driven by mixing amphiphilic peptides with increasing amounts of DNA-pep chimeras.

how such gradual changes in structures may come about during simple mixing processes, we have further followed structure formation in N_3-pep solutions that were gradually seeded with increasing amounts of dsCon. AFM images (Figure S13) indeed show the same trend as observed for the assembly of the corresponding individual mixtures (Figure 3). Control experiments, carried out by simply mixing solutions of dsDNA and N_3-pep, did not result the same structural changes, but rather the formation of simple fibril or tape-like architectures (Figure S14).

We propose that each of the new architectures could find utility in the future; for example, the stiff linear fibrils formed in the dsCon/pep mixtures might be useful for molecular electronics,[17] while the dsCon spheres could serve as efficient hosts for binding and releasing small molecules (vide infra). Aggregation of dsCon into spherical structures with concentric bilayers induces the encapsulation of the hybridized DNA segments and can thus confer additional duplex stability, namely, minimize denaturation of dsDNA unless harsh conditions are applied. This hypothesis was tested in thermal denaturation experiments performed by following the changes in UV absorption at 260 nm upon heating and transition of the DNA duplex into single strands (Figure 5a and Table S1). The results

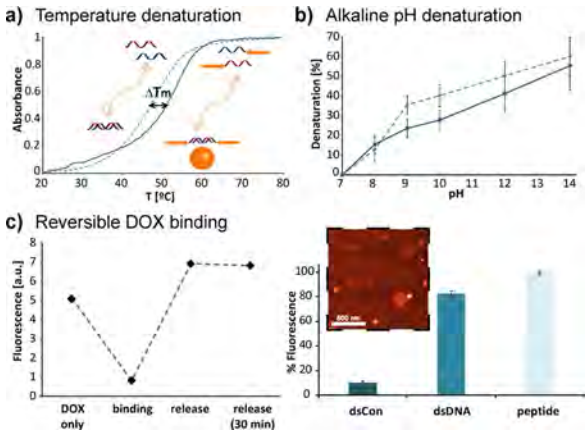

Figure 5. Stability and binding properties of the dsCon spherical structures. a, b) Temperature-dependent and pH-dependent denaturation. In each panel, the dsCon denaturing stability (solid line) is compared to that of dsDNA (dashed line). c) Left: Fluorescence measurements (590 nm) reflecting the quenching and restoration of emission, upon binding of Dox to dsCon and its release, respectively. Right: Dox fluorescence upon binding to dsCon, dsDNA and N_3-pep assemblies (Figure S18); 100% fluorescence was calibrated for the free Dox emission. Inset: AFM images of dsCon spheres after DOX intercalation.

show a duplex melting temperature (T_m) for mixtures containing dsCon that is about 6 °C higher than that of the control unmodified dsDNA. Subsequently, stability studies were also performed to probe the chemical (alkaline-pH-dependent) denaturation of dsCon. At an alkaline pH, the activity of OH^- groups causes denaturation of DNA duplexes by removing the protons involved in H-bond formation from the guanine and thymine bases.[18] Duplex denaturation as a function of pH was followed, and the denaturation fractions calculated as previously reported (see the Supporting Information).[19] A markedly lower degree of duplex denaturation was observed for dsCon than for dsDNA above pH 8 (Figure 5b). AFM investigation confirmed that dsCon spheres can be readily formed at pH 8 and that they are disrupted at pH $\geq$ 10 (Figure S16).

NA-pep conjugates[20] and peptide nucleic acid (PNA)[21] oligomers have mostly been utilized as soluble entities with applications in the medical sciences, for example, for drug delivery or gene silencing. Little is known about the binding properties of NA-pep conjugate assemblies, which could serve as (drug) carriers or as catalysts for reactions of encapsulated substrates.

Therefore, we tested the dsCon spheres as binders for known peptide fibril and dsDNA intercalators. Binding of ThT to β-sheet-rich structures or to DNA[22] induces a characteristic red-shift in its fluorescence spectrum, enhancing the emission at around 480 nm. A binding assay, performed by mixing 100 μM ThT with 10 μM dsCon, revealed significant staining of the dsCon spheres (Figure S17). Remarkably, the increase in ThT fluorescence upon binding to dsCon was higher than that observed in control experiments, in which we followed ThT binding to dsDNA, N_3-pep, or even to the mixture of both dsDNA and N_3-pep (Figure S17). These findings indicate that the dsCon sphere interior might provide additional binding sites to encapsulate the ThT.

The binding of dsCon spheres to the Doxorubicin (Dox) molecule, a DNA intercalator often used for cancer chemotherapy, was then analyzed by following the quenching of Dox auto-fluorescence upon mixing with dsCon. Studies at a 1:1 host/drug molar ratio (10 μM each) showed almost complete fluorescence quenching, attributed to Dox binding to and within dsCon structures (Figure 5c). Evidence for the reversible nature of this binding was obtained by adding the denaturing agent guanidinium chloride to a mixture of Dox and dsCon (1:1); the denaturing agent caused immediate Dox release, as observed by the restoration of maximal fluorescence (Figure 5c, left). We therefore suggest that this system might be useful for future controlled drug-delivery applications. Structural characterization by AFM of Dox-binding dsCon revealed that the spheres expanded substantially to accommodate the bound aromatic entities (Figure 5c, inset). In addition, our results showed that mixing 10 μM dsCon with a large (10-fold) excess of Dox did not induce a significant change in Dox auto-fluorescence, probably because the dsCon structures were already saturated with Dox. This notion is further supported by the mixture AFM images, showing fibril like structures, as also observed for Dox molecules alone (Figure S19). Control binding experiments showed a small change due to Dox binding to dsDNA and no quenching upon mixing of Dox with the peptide fibrils (Figure 5c, right). Here, we again attribute the stronger Dox binding to dsCon to additional binding sites provided by the DsCon self-assembly, as does the slower Dox release back into the solution.

Conclusions

We have revealed a variety of supramolecular structures emerging in mixtures of amphiphilic peptides and DNA-pep chimeras. The assemblies formed by the double-stranded chimera confer higher stability on the DNA duplex and bind to small molecule substrates better than their NA or peptide moieties alone. We accordingly suggest that these molecules, or similar conjugates, could serve as new materials for various applications, such as catalysis, electron transfer and drug delivery. Furthermore, we propose that our research might offer a new understanding of early chemical evolution, towards the origin of life. Since it has recently been shown that both peptide and nucleic acid precursors can be formed in a prebiotic environment from simple building blocks of unified origin,[23] we suggest that synergistic activity such as that demonstrated here may have led to the selection of functional chimeras. Together with other recent results demonstrating structural and functional synergy in NA-pep systems[3c,24] and also synergy between simple prebiotically relevant molecules from different families, such as NA-lipid,[13,25] pep-lipid,[26] and sugar-pep,[27] the current study shows the rapid progression in complexity and systems chemistry[28,29] that would have facilitated a large repertoire of functions.

Experimental Section

General

Chemical and reagents were purchased from Aldrich or Merck and unless otherwise specified used without further purification. Amino acids, resins and coupling reagents were purchased from Novabiochem and Alfa Aesar, and DMF was purchased from Biotech Grade. 5′ hexynyl modified oligonucleotides were purchased from Bio-Synthesis, Inc. Doxorubicin was generously provided by Prof. Ayelet David, School of Pharmacy, Ben-Gurion University of the Negev.

Azide-modified peptide synthesis

Triflyl azide, used for modification of amine at the N terminus or side chain was synthesized as follows: a suspension of sodium azide (3.3 mmol) in 4 mL of pyridine was cooled in an ice bath. Then triflic anhydride (2.78 mmol) was added to the mixture by a syringe during 5 min of stirring. After the reaction had been maintained for 2 h in the ice bath, the TfN_3-containing solution (after filtration of the salts) was added to the amine solution for subsequent diazo transfer reaction. In parallel, the free amine peptide sequence was synthesized at 0.1–0.2 mmol scale on a Rink amide MBHA resin using standard Fmoc protocols. Thereafter, 100 mg of peptide-attached resin was allowed to swell in DMF for 20 min, followed by the addition of 0.02 mmol of $CuSO_4$ in MeOH (1 mL) and triethylamine (0.02 mol). The mixture was cooled in the ice bath for a few minutes, and then the solution of triflyl azide in pyridine was added dropwise. The reaction mixture was allowed to warm to room temperature and reacted for 5 h. The same procedure was repeated 3 times with fresh reagents. Upon completion, the reaction mixture was washed with DMF, DIPEA/DMF (99.5:0.5, 3× 2 min), and finally with DMF, DCM and ether. The azido-peptide was obtained after cleavage and global deprotection with a mixture of TFA/TIS/water (95:2.5:2.5). The resin was removed by filtration under reduced pressure and the TFA was evaporated out of the peptide mixture. Cold ether, 8–10 times in volume, was added to precipitate the crude peptide. The peptide was purified by preparative HPLC using a Dionex Ultimate 3000 instrument with C18 reverse phase preparative column at a flow rate of 20 mL min^{-1}. The identity and purity of the peptide were analyzed on a Dionex 1100 using a reverse phase C18 column at a flow rate of 1.5 mL min^{-1}. ESI-MS mass spectrometry (LCMS Thermo Surveyor 355) analysis was performed to verify the molecular weight (measured Mw = 1143).

Synthesis of DNA-peptide conjugates via "click" chemistry

The azido-peptide (1 equiv) and 5′ hexynyl DNA (1 equiv.) were dissolved in water/*t*BuOH (1:1). $CuSO_4$ (1% mole equiv) and TBTA (5% mole equiv) were added to the solution, followed by sodium ascorbate (0.5 equiv). The mixture was shaken at 37 °C. The reaction

progress was monitored by analytical HPLC on a Dionex 1100 using a reverse phase C18 column; upon completion, the product was purified by HPLC, and analyzed by HPLC and MALDI-TOF mass spectrometry (Figures 1 and S1).

Sample preparation for biophysical studies

Aqueous solutions of the chosen sample were prepared fresh, by dissolving lyophilized powder in phosphate buffer (10 mM), pH ≈7. Peptide containing samples were dissolved by sonication for 10 min. After sonication, the samples were vortexed to eliminate any undesired structures originating from the sonication, and then equilibrated for at least 2 hours. Samples containing dsDNA and dsCon were incubated at elevated temperatures (>70 °C) for 10 min, cooled down to RT and then equilibrated for at least three more hours.

The concentrations of peptide stock solutions were determined by measuring the UV absorption of a diluted peptide stock solution at 257 nm (the maximum absorption of phenylalanine). Concentrations of DNA and DNA-pep samples were determined by measuring the UV absorption of a diluted stock solution at 260 nm (the maximum absorption of DNA), using $\varepsilon = 99\,000$ L/(mole*cm) for DNA1 and $\varepsilon = 85400$ L/(mole*cm) for DNA2.

Circular dichroism measurements

CD spectra were performed on a Jasco J-815 CD-spectrometer. All samples were prepared by dissolving powder of peptide, DNA or conjugates in the phosphate buffer, and re-checking the concentration by UV-absorption. CD spectrum between 200 nm to 320 nm was recorded with data steps of 0.5 nm, a scan speed of 10 nm min^{-1}, response time 4 s and a bandwidth of 2 nm. The baseline buffer spectrum was measured and subtracted from the sample spectra. All samples were measured in triplicate, and the results were averaged automatically.

Atomic force microscopy (AFM) imaging

Samples were prepared with an addition of 10 mM $MgCl_2$, for better binding of negatively charged compounds to the mica surfaces. A 3 μL aliquot of solution after equilibration as described above was deposited on a freshly cleaved mica surface. The sample was then slowly dried in air overnight. Topography images were acquired by AFM (SolverPro, NT-MDT, Ru) in tapping mode using noncontact tips BudgetSensors Multi75Al-G, 3 N m^{-1}, 75 kHz. Image processing, which included second order polynomial line fitting and cross-section analysis, was done using the NOVA AFM software. AFM histograms of height distribution (Figure S7) were prepared by counting 25 different AFM features.

Cryogenic transmission electron microscopy (Cryo-TEM) imaging

Samples for direct imaging of the aqueous dispersions were prepared in the controlled environment box of a vitrification robot (Vitrobot, FEI), as follows: a 5 μL drop of the sample solution was deposited on a glow-discharged TEM grid, the excess liquid was automatically blotted with a filter paper, and the specimen was rapidly plunged into liquid ethane and transferred to liquid nitrogen, where it was kept until use. The samples were examined below −175 °C using an FEI Tecnai 12 G^2 TWIN TEM that operated at 120 kV in low-dose mode and with a few micrometers under focus to increase the phase contrast. The images were recorded with a Gatan charge-coupled device camera (model 794). The images of the assemblies were analyzed by Digital Micrograph software (Version 3.1).

Statistical analysis based on the Cryo-TEM data

Hundred individual spherical objects were measured, and the diameter of each one was determined as the average of 3 individual lines that pass through the sphere center (Figure S9). Differential count analysis of all the measured diameters was obtained using the Excel statistical COUNTIF function, by utilizing the following bins: 0.5, 1 and 2. The value range screened by the COUNTIF function included all the 100 sphere diameters, and the criteria applied as higher or equal given bin, but smaller than the next bin. For example, for bin = 0.5 and diameter = 24, the function assigned the number of measured objects with diameters equal to or greater than 24 nm, but lower than 24.5 nm. For all three analyzed bin values, we have clearly observed higher counts for diameters divisible by 6, correlating well with the theoretical cross section of a single DNA-pep layer (Figure 4 in the main manuscript), which may suggest that the assembly of each layer adds ≈6 nm to the sphere diameter.

Transmission electron microscopy (TEM) imaging

A TEM copper grid with a 200-mesh carbon support (Electron Microscopy Sciences) was covered with 10 μL of a peptide solution (1 mM) in 10 mM phosphate buffer pH 7, for 1 min before wicking the excess solution with filter paper. 10 μL of the staining solution, 2% uranyl acetate, (Sigma–Aldrich), was added and incubated for 2 min; excess solution was wicked away, and the grids were placed in desiccators to dry under vacuum. A Hitachi H-7500 transmission electron microscope was used to image the samples at 75 kV.

Attenuated total reflectance Fourier transform infrared spectroscopy (ATR-FTIR)

Aliquot (10 μL) of peptide solution was dried as thin films on an ATR diamond crystal. FT-IR spectra were acquired using a FTIR Spectrometer 6700 at room temperature, and averaging 512 scans with 2 cm^{-1} resolution, using a sensitive liquid N_2 cooled MCT-A detector with a 5-mm aperture and a scanning speed of 4 mm sec^{-1}.

Dynamic light scattering (DLS) measurements

Samples were prepared at 50 μM and 500 μM concentrations in phosphate buffer (pH 7) and transferred to a cylindrical glass ampoule (length ca. 8 cm; diameter ca. 0.8 cm) of high quality optical glass. It was then placed in a vat filled with toluene as the index matching fluid. During the course of the measurements, the vat was kept at room temperature. The light source was an argon ion laser and photons scattered by the sample were collected by a photomultiplier tube mounted on the goniometer arm at 90° to the direction of the incident radiation. Measurements were acquired using a CGS-3 LSE-5004 correlator at room temperature.

Fluorescence measurement of thioflavin T (ThT) staining

Samples used for the measurements contained a total concentration of 10 μM of peptide, dsDNA or dsCon, in a volume of 70 μL of 10 mM phosphate buffer pH 7. Samples containing dsDNA and dsCon were first incubated at elevated temperatures (≥70 °C) for 10 min, then 100 μM ThT was added, and the spectra were measured. Fluorescence spectra were recorded on a 3001 Thermo Vari-

oSkan fluorescence spectrometer, equipped with a 96-microwell-plate reader. ThT Spectra were collected from 465 to 700 nm, using an excitation wavelength of 440 nm (excitation slit width: 12 nm), at scan speed of 100 nm min^{-1}. The baseline of 100 μM thioflavin T in the buffer was subtracted from the sample spectra. Fluorescence emission signals at 480 nm were used to compare ThT binding to the different assemblies.

Fluorescence measurement of doxorubicin (Dox)

Samples containing a total concentration of 0–25 μM of peptide, dsDNA or dsCon in a volume of 70 μL, were prepared in 10 mM phosphate buffer pH 7. Samples containing dsDNA and dsCon were incubated at elevated temperatures ($\geq$70 °C) for 10 min, then 10 μM Doxorubicin was added, and spectra were recorded on a 3001 Thermo VarioSkan fluorescence spectrometer, equipped with a 96-microwellplate reader. Spectra of doxorubicin were collected from 505 to 700 nm, using an excitation wavelength of 480 nm (excitation slit width: 12 nm), and scan speed of 100 nm min^{-1}. The intensity of fluorescence signals at 590 nm was used to compare Dox binding to the different assemblies; the values are shown as normalized emission percentage, using the signal of free Dox in buffer as 100% emission.

Dictating the double stranded DNA species melting temperatures

The samples used for the thermal melting analysis contained a total concentration of 5 μM, with **DNA1-pep** and **DNA2-pep** in 1:1 ratio in a total volume of 200 μL. The samples were prepared in 10 mM phosphate buffer pH 7 containing 50 mM Na_2SO_4. dsDNA solutions of the same concentrations were used as a control. T_m was found using the change in absorption at 260 nm upon transition from duplex to single strands. The scans were performed on an Agilent Cary 60 UV/Vis spectrometer with Temperature Controller TC125 using a cuvette of 1 cm pass length. For the melting and annealing measurements, first the sample was heated fast to 80 °C and incubated for 10 min, before cooling down to 20 °C at a rate of 0.5 °C min^{-1}. The sample was kept at 20 °C for 10 min, before heating back up to 80 °C at the same rate. The absorbance values were normalized using the given in Equation (1):

$$\text{Normalized value} = \frac{\text{Abs} - \text{Abs}_0}{\text{Abs}_{max} - \text{Abs}_0} \quad (1)$$

The T_m was found by determining the maximum of the first derivatives of absorbance signals resulting from three separate melting and annealing measurements.

Analyzing the pH-dependent denaturation of double stranded DNA species

NaOH (1 M) solution was used to denature the DNA in dsCon and dsDNA assemblies. NaOH solution was slowly added to 200 μL dsCon or dsDNA solutions, in order to obtain incremental one-unit jumps in the solution pH. The mixture was homogenized with continuous pipetting and vortex, after which the final absorbance (A_{260}) was measured using the UV/Vis spectrophotometer. The changes in 260 nm absorbance as a function of the pH were applied to calculate the denaturation percentage,[1] using a simplified equation. Variables measured and used in the equation include: Initial A_{260}, Final A_{260} and Blank A_{260} [Eq. (2)].

$$\text{Denaturation } (\%) = \left(\frac{\text{Final } A_{260} - \text{Blank } A_{260}}{\text{Initial } A_{260}} - 1\right) \text{x200} \quad (2)$$

The results presented in the manuscript (Figure 5) are the mean values obtained for 3 repetitions of the experiment and the standard deviations.

Acknowledgements

This research is sponsored by an NSF-BSF grant (2015671). We also acknowledge support from the COST actions CM1304 and TD1308. We thank Prof. N. Ashkenasy (BGU) and Prof. D. G. Lynn (Emory University) for fruitful discussions.

Conflict of interest

The authors declare no conflict of interest.

Keywords: nanostructures · nucleic acids · peptide conjugates · systems chemistry

[1] A. Yonath, *Angew. Chem. Int. Ed.* **2010**, *49*, 4340–4354; *Angew. Chem.* **2010**, *122*, 4438–4453.
[2] J. D. Perlmutter, M. F. Hagan, *Annu. Rev. Phys. Chem.* **2015**, *66*, 217–239.
[3] a) J. T. Goodwin, A. K. Mehta, D. G. Lynn, *Acc. Chem. Res.* **2012**, *45*, 2189–2199; b) A. Brack, *Chem. Biodiversity* **2007**, *4*, 665–679; c) A. N. Lazar, A. W. Coleman, S. Terenzi, P. Strazewski, *Chem. Commun.* **2006**, 63–65.
[4] a) L. Adler-Abramovich, E. Gazit, *Chem. Soc. Rev.* **2014**, *43*, 6881–6893; b) M. Reches, E. Gazit, *Curr. Nanosci.* **2006**, *2*, 105–111; c) S. Fleming, R. V. Ulijn, *Chem. Soc. Rev.* **2014**, *43*, 8150–8177; d) M. J. Webber, E. J. Berns, S. I. Stupp, *Isr. J. Chem.* **2013**, *53*, 530–554; e) S. Cavalli, F. Albericio, A. Kros, *Chem. Soc. Rev.* **2010**, *39*, 241–263; f) Y. Gao, F. Zhao, Q.-G. Wang, Y. Zhang, B. Xu, *Chem. Soc. Rev.* **2010**, *39*, 3425–3433; g) C. A. E. Hauser, S. Zhang, *Chem. Soc. Rev.* **2010**, *39*, 2780–2790; h) J. M. A. Carnall, C. A. Waudby, A. M. Belenguer, M. C. A. Stuart, J. J. P. Peyralans, S. Otto, *Science* **2010**, *327*, 1502–1506; i) N. Singh, M. Kumar, J. F. Miravet, R. V. Ulijn, B. Escuder, *Chem. Eur. J.* **2017**, 981–993.
[5] a) Y. Raz, B. Rubinov, M. Matmor, H. Rapaport, G. Ashkenasy, Y. Miller, *Chem. Commun.* **2013**, *49*, 6561–6563; b) H. Rapaport, K. Kjaer, T. R. Jensen, L. Leiserowitz, D. A. Tirrell, *J. Am. Chem. Soc.* **2000**, *122*, 12523–12529; c) H. Rapaport, *Supramol. Chem.* **2006**, *18*, 445–454.
[6] M. Tena-Solsona, J. Nanda, S. Diaz-Oltra, A. Chotera, G. Ashkenasy, B. Escuder, *Chem. Eur. J.* **2016**, *22*, 6687–6694.
[7] a) B. Rubinov, N. Wagner, H. Rapaport, G. Ashkenasy, *Angew. Chem. Int. Ed.* **2009**, *48*, 6683–6686; *Angew. Chem.* **2009**, *121*, 6811–6814; b) B. Rubinov, N. Wagner, M. Matmor, O. Regev, N. Ashkenasy, G. Ashkenasy, *ACS Nano* **2012**, *6*, 7893–7901.
[8] a) D. Ivnitski, M. Amit, B. Rubinov, R. Cohen-Luria, N. Ashkenasy, G. Ashkenasy, *Chem. Commun.* **2014**, *50*, 6733–6736; b) D. Ivnitski, M. Amit, O. Silberbush, Y. Atsmon-Raz, J. Nanda, R. Cohen-Luria, Y. Miller, G. Ashkenasy, N. Ashkenasy, *Angew. Chem. Int. Ed.* **2016**, *55*, 9988–9992; *Angew. Chem.* **2016**, *128*, 10142–10146.
[9] a) N. Venkatesan, B. H. Kim, *Chem. Rev.* **2006**, *106*, 3712–3761; b) K. Lu, Q. P. Duan, L. Ma, D. X. Zhao, *Bioconjugate Chem.* **2010**, *21*, 187–202.
[10] S. Yuran, Y. Razvag, M. Reches, *ACS Nano* **2012**, *6*, 9559–9566.
[11] a) C. Lou, M. C. Martos-Maldonado, C. S. Madsen, R. P. Thomsen, S. R. Midtgaard, N. J. Christensen, J. Kjems, P. W. Thulstrup, J. Wengel, K. J. Jensen, *Nat. Commun.* **2016**, *7*, 12294–12302; b) J. Kypr, I. Kejnovská, D. Renčiuk, M. Renčiuk, *Nucl. Acids Res.* **2009**, *37*, 1713–1725.
[12] Y. Mai, A. Eisenberg, *Chem. Soc. Rev.* **2012**, *41*, 5969–5985.
[13] R. S. Shirazi, K. K. Ewert, B. F. B. Silva, C. Leal, Y. Li, C. R. Safinya, *Langmuir* **2012**, *28*, 10495–10503.

[14] a) X. Li, Y. Kuang, H. C. Lin, Y. Gao, J. Shi, B. Xu, *Angew. Chem. Int. Ed.* **2011**, *50*, 9365 – 9369; *Angew. Chem.* **2011**, *123*, 9537 – 9541; b) N. Gour, J. N. Abraham, M. Chami, A. Castillo, S. Verma, C. Vebert-Nardin, *Chem. Commun.* **2014**, *50*, 6863 – 6865; c) P. Liu, R. Ni, A. K. Mehta, W. S. Childers, A. Lakdawala, S. V. Pingali, P. Thiyagarajan, D. G. Lynn, *J. Am. Chem. Soc.* **2008**, *130*, 16867 – 16869; d) R. M. Turk-MacLeod, D. Puthenvedu, I. Majerfeld, M. Yarus, *J. Mol. Evol.* **2012**, *74*, 217 – 225.

[15] a) J. E. Noble, E. De Santis, J. Ravi, B. Lamarre, V. Castelletto, J. Mantell, S. Ray, M. G. Ryadnov, *J. Am. Chem. Soc.* **2016**, *138*, 12202 – 12210; b) M. Kye, Y.-b. Lim, *Angew. Chem. Int. Ed.* **2016**, *55*, 12003 – 12007; *Angew. Chem.* **2016**, *128*, 12182 – 12186; c) W. M. Aumiller, Jr., C. D. Keating, *Nat. Chem.* **2016**, *8*, 129 – 137.

[16] a) R. Ni, Y. Chau, *J. Am. Chem. Soc.* **2014**, *136*, 17902 – 17905; b) R. Ni, Y. Chau, *Angew. Chem. Int. Ed.* **2017**, *56*, 9356 – 9360; *Angew. Chem.* **2017**, *129*, 9484 – 9488; c) T. Jiang, T. A. Meyer, C. Modlin, X. Zuo, V. P. Conticello, Y. Ke, *J. Am. Chem. Soc.* **2017**, *139*, 14025 – 14028.

[17] M. Mizrahi, A. Zakrassov, J. Lerner-Yardeni, N. Ashkenasy, *Nanoscale* **2012**, *4*, 518 – 524.

[18] S. Shin, L. A. Day, *Anal. Biochem.* **1995**, *226*, 202 – 206.

[19] a) X. F. Wang, A. Son, *Environmental Science-Processes Impacts* **2013**, *15*, 2204 – 2212; b) X. Wang, H. J. Lim, A. Son, *Environ. Health Toxicol.* **2014**, *29*, e2014007.

[20] a) D. M. Copolovici, K. Langel, E. Eriste, U. Langel, *ACS Nano* **2014**, *8*, 1972 – 1994; b) J. J. Turner, G. D. Ivanova, B. Verbeure, D. Williams, A. A. Arzumanov, S. Abes, B. Lebleu, M. J. Gait, *Nucl. Acids Res.* **2005**, *33*, 6837 – 6849; c) T. P. Wang, N. C. Ko, Y. C. Su, E. C. Wang, S. Severance, C. C. Hwang, Y. T. Shih, M. H. Wu, Y. H. Chen, *Bioconjugate Chem.* **2012**, *23*, 2417 – 2433.

[21] T. Shiraishi, P. E. Nielsen, *Methods Mol. Biol.* **2014**, *1050*, 193 – 205.

[22] A. Biancardi, T. Biver, A. Burgalassi, M. Mattonai, F. Secco, M. Venturini, *Phys. Chem. Chem. Phys.* **2014**, *16*, 20061 – 20072.

[23] B. H. Patel, C. Percivalle, D. J. Ritson, C. D. Duffy, J. D. Sutherland, *Nat. Chem.* **2015**, *7*, 301 – 307.

[24] a) R. Wieczorek, M. Doerr, A. Chotera, P. L. Luisi, P.-A. Monnard, *ChemBioChem* **2013**, *14*, 217 – 223; b) J. E. Hein, E. Tse, D. G. Blackmond, *Nat. Chem.* **2011**, *3*, 704 – 706; c) H. Griesser, M. Bechthold, P. Tremmel, E. Kervio, C. Richert, *Angew. Chem. Int. Ed.* **2017**, *56*, 1224 – 1228; *Angew. Chem.* **2017**, *129*, 1244 – 1248; d) H. Griesser, P. Tremmel, E. Kervio, C. Pfeffer, U. E. Steiner, C. Richert, *Angew. Chem. Int. Ed.* **2017**, *56*, 1219 – 1223; *Angew. Chem.* **2017**, *129*, 1239 – 1243; e) Y. Ura, J. M. Beierle, L. J. Leman, L. E. Orgel, M. R. Ghadiri, *Science* **2009**, *325*, 73 – 77.

[25] M. C. Wamberg, R. Wieczorek, S. B. Brier, J. W. de Vries, M. Kwak, A. Herrmann, P.-A. Monnard, *Bioconjugate Chem.* **2014**, *25*, 1678 – 1688.

[26] a) S. Murillo-Sanchez, D. Beaufils, J. M. Gonzalez Manas, R. Pascal, K. Ruiz-Mirazo, *Chem. Sci.* **2016**, *7*, 3406 – 3413; b) E. C. Izgu, A. Björkbom, N. P. Kamat, V. S. Lelyveld, W. Zhang, T. Z. Jia, J. W. Szostak, *J. Am. Chem. Soc.* **2016**, *138*, 16669 – 16676; c) H. R. Marsden, I. Tomatsu, A. Kros, *Chem. Soc. Rev.* **2011**, *40*, 1572 – 1585.

[27] A. J. Wagner, D. Y. Zubarev, A. Aspuru-Guzik, D. G. Blackmond, *ACS Cent. Sci.* **2017**, *3*, 322 – 328.

[28] G. Ashkenasy, T. M. Hermans, S. Otto, A. F. Taylor, *Chem. Soc. Rev.* **2017**, *46*, 2543 – 2554.

[29] Y. Bai, A. Chotera, O. Taran, C. Liang, G. Ashkenasy, D. G. Lynn, *Chem. Soc. Rev.* **2018**, DOI: https://doi.org/10.1039/C8CS00174J.

Manuscript received: February 12, 2018
Revised manuscript received: March 29, 2018
Accepted manuscript online: May 4, 2018
Version of record online: June 14, 2018